Journal of Materials Chemistry A

PAPER

View Article Online
View Journal | View Issue

Cite this: J. Mater. Chem. A, 2019, 7, 3128

A metal–organic framework with suitable pore size and dual functionalities for highly efficient post-combustion CO_2 capture†

Hui-Min Wen,[a] Caijun Liao,[a] Libo Li,[bc] Ali Alsalme,[d] Zeid Alothman,[d] Rajamani Krishna,[e] Hui Wu,[f] Wei Zhou,*[f] Jun Hu*[a] and Banglin Chen*[b]

Received 3rd December 2018
Accepted 14th January 2019

DOI: 10.1039/c8ta11596f

rsc.li/materials-a

Capturing carbon dioxide (CO_2) from flue gases with porous materials has been considered as a viable alternative technology to replace traditional liquid amine adsorbents. A large number of microporous metal–organic frameworks (MOFs) have been developed as CO_2-capturing materials. However, it is challenging to target materials with both extremely high CO_2 capture capacity and gas selectivity (so-called trade-off) along with moderate regeneration energy. Herein, we developed a novel porous material, $[Cu(dpt)_2(SiF_6)]_n$ (termed as UTSA-120; dpt = 3,6-di(4-pyridyl)-1,2,4,5-tetrazine), which is isoreticular to the net of SIFSIX-2-Cu-i. This material exhibits simultaneously high CO_2 capture capacity (3.56 mmol g^{-1} at 0.15 bar and 296 K) and CO_2/N_2 selectivity (~600), both of which are superior to those of SIFSIX-2-Cu-i and most other MOFs reported. Neutron powder diffraction experiments reveal that the exceptional CO_2 capture capacity at the low-pressure region and the moderate heat of CO_2 adsorption can be attributed to the suitable pore size and dual functionalities ($SiF6^{2-}$ and tetrazine), which not only interact with CO_2 molecules but also enable the dense packing of CO_2 molecules within the framework. Simulated and actual breakthrough experiments demonstrate that UTSA-120a can efficiently capture CO_2 gas from the CO_2/N_2 (15/85, v/v) and CO_2/CH_4 (50/50) gas mixtures under ambient conditions.

Introduction

The concentration of atmospheric carbon dioxide (CO_2) has sharply risen from 278 ppm at the beginning of the industrial revolution to >400 ppm today, which causes global climate change.[1,2] Efforts to reduce the increase in atmospheric CO_2 concentrations rely on the development of economical methods to capture CO_2 from flue gases and the atmosphere.[3] The current state-of-the-art capture technology is to use liquid amine chemisorbents; however, chemisorbents typically suffer from the corrosive nature of solvents, fouling of process equipment, and high energy cost for solvent regeneration. Physical adsorption based on porous materials offers promise to address the above problems. Compared with chemisorbents for complete CO_2 capture from flue gases, the CO_2 adsorption on porous materials is "physical" and weak, making these adsorbents relatively low in selectivity. Thus, physisorptive selectivity is an important parameter for evaluating these solid adsorbents' performance. Recent studies show that the cost for CO_2 capture from flue gases can be significantly reduced if the CO_2/N_2 selectivity is enhanced above 500 for an adsorbent with a CO_2 uptake capacity higher than 4 mmol g^{-1}.[4] Therefore, both high CO_2 adsorption uptake and CO_2/N_2 selectivity are required for ideal CO_2-capturing adsorbents.

Microporous metal–organic frameworks (MOFs) represent an emerging type of porous materials as promising adsorbents for carbon capture due to their easily tunable structure, pore size, and functionality.[5–7] Tremendous efforts have been dedicated to develop MOFs with high CO_2 adsorption capacity or separation selectivity.[8–10] Incorporation of functional sites and fine-tuning of pore sizes/shapes in MOFs are two powerful strategies for this purpose.[11–15] However, it is still challenging to target materials with extremely high CO_2 capture capacity/selectivity and moderate CO_2 enthalpy of adsorption simultaneously. For example, the

[a]College of Chemical Engineering, Zhejiang University of Technology, Chaowang Road #18, Hangzhou 310014, Zhejiang, China. E-mail: hjzjut@zjut.edu.cn

[b]Department of Chemistry, University of Texas at San Antonio, One UTSA Circle, San Antonio, Texas 78249-0698, USA. E-mail: banglin.chen@utsa.edu; Fax: +1)-210-458-7428

[c]College of Chemistry and Chemical Engineering, Taiyuan University of Technology, Taiyuan 030024, Shanxi, China

[d]Chemistry Department, College of Science, King Saud University, P O Box 2455, Riyadh 11451, Saudi Arabia

[e]Van't Hoff Institute for Molecular Sciences, University of Amsterdam, Science Park 904, 1098 XH Amsterdam, Netherlands

[f]NIST Center for Neutron Research, National Institute of Standards and Technology, Gaithersburg, MD 20899-6102, USA. E-mail: wzhou@nist.gov

† Electronic supplementary information (ESI) available: PXRD, crystal data, adsorption isotherms and structure refinement for UTSA-120a and UTSA-120a·2.6CO_2. CCDC 1881280 and 1882294. For ESI and crystallographic data in CIF or other electronic format see DOI: 10.1039/c8ta11596f

MOF-74 series has a high density of open metal sites that drive a record high CO_2 uptake but displays moderately high selectivities (40–140).[8] Some ultra-microporous MOFs exhibit full molecular sieving and then record separation selectivity but relatively low uptake of CO_2 at 0.15 bar (1.5–2.4 mmol g^{-1}) due to the small pore sizes.[13,14] The alkylamino-functionalization within MOFs can improve both low-pressure CO_2 adsorption selectivity and capacity with high enthalpy of CO_2 adsorption (70–110 kJ mol^{-1}).[15]

Recent studies have shown that the SIFSIX series (SIFSIX = hexafluorosilicate (SiF_6^{2-})) are very promising candidates for CO_2-capturing adsorbents, because their pore size can be finely tuned and SiF_6^{2-} anions have moderately strong interactions with CO_2.[13,16] Among the reported SIFSIX materials, the interpenetrated SIFSIX-2-Cu-i exhibits exceptional CO_2 uptake under ambient conditions, and moderately high CO_2/N_2 selectivity (140) and CO_2 heat of adsorption.[4b] Reducing the pore size to ~3.5 Å in pyrazine-based SIFSIX-3 materials can afford full molecular sieving toward CO_2/N_2 separation and thus the record selectivity.[13] However, the extremely small pore space delimits the total CO_2 uptake at 0.15 bar and the ultra-strong interactions with CO_2 in SIFSIX-3 offer relatively high regeneration energy. Evidently, simple control of the pore size in SIFSIX materials is not the best choice to target ideal materials for CO_2 capture from flue gases. We speculated that if we introduce secondary functional groups into the framework of SIFSIX-2-Cu-i to enhance the interactions with CO_2 molecules, the resulting material would have an increased CO_2 uptake at the low-pressure region, thus achieving both higher CO_2 capture capacity (especially at 0.15 bar) and selectivity.

Our experimental and simulation studies verify this hypothesis, and we herein used a functionalized organic linker of 3,6-di(4-pyridyl)-1,2,4,5-tetrazine (dpt) instead of 4,4′-dipyridylacetylene (dpa) to construct isoreticular UTSA-120 (Fig. 1). The resulting material shows a similar pore size to SIFSIX-2-Cu-i but has dual functionalities (SiF_6^{2-} and tetrazine) decorated on the pore surfaces. As expected, UTSA-120a exhibits simultaneously high CO_2 adsorption capacity (3.56 mmol g^{-1} at 0.15 bar and 296 K) and CO_2/N_2 selectivity (~600), both of which are among the highest reported for MOF materials. In addition, UTSA-120a also shows notably lower heat of adsorption (Q_{st}) for CO_2 (27–31 kJ mol^{-1}) compared to the benchmark SIFSIX-3 (50–55 kJ mol^{-1}) and liquid amines (~105 kJ mol^{-1}). This rare combination of exceptional CO_2 adsorption capacity, high CO_2/N_2 selectivity and moderate Q_{st} in UTSA-120a is mainly due to the suitable pore size and functionality conformation created by SiF_6^{2-} and tetrazine that enable the optimal packing of CO_2 within pore channels. Highly efficient capture of CO_2 from CO_2/N_2 (15/85) and CO_2/CH_4 (50/50) mixtures was confirmed by simulated and experimental breakthrough studies.

Results and discussion

The reaction of dpt with $CuSiF_6$ in methanol/water solution at room temperature for 1 day afforded a pink powder sample of $[Cu(dpt)_2(SiF_6)]_n$ (UTSA-120). The PXRD patterns of the as-synthesized and fully activated UTSA-120 are shown in Fig. S1 (ESI†). The diffraction peak positions remain unchanged before and after sample activation, indicating that the UTSA-120 framework is robust upon guest removal. The PXRD patterns can be indexed to the tetragonal *I*4/mmm space group, the same as that of SIFSIX-2-Cu-i. Despite extensive attempts, we were not able to obtain single crystals large enough for single-crystal X-ray diffraction studies. Therefore, we used neutron diffraction to determine the detailed structure of activated UTSA-120a. High-resolution neutron diffraction data were collected at room temperature, and Rietveld structural refinement was performed (Fig. S2, ESI†).[17] The obtained detailed structural information of UTSA-120a is provided in Table S1 (ESI†).

As depicted in Fig. 1, structural analysis revealed that UTSA-120a is composed of doubly interpenetrated nets that are isostructural to the nets in SIFSIX-2-Cu-i. The use of the longer dpt instead of dpa as a linker offers a slightly larger pore size (4.6 Å) in UTSA-120a than that in SIFSIX-2-Cu-i (4.4 Å). Most importantly, the incorporated tetrazine rings are decorated around the pore channels, and all the Lewis basic N sites point into the pores. Previous studies have well documented that functional SiF_6^{2-} or uncoordinated N-sites could effectively enhance the gas-binding affinity with CO_2.[18] Thus, the synergistic effect of dual functionalities in UTSA-120a may lead to enhanced interactions with CO_2 molecules as compared to SISXIF-2-Cu-i, thus achieving higher CO_2 capture and separation capacities.

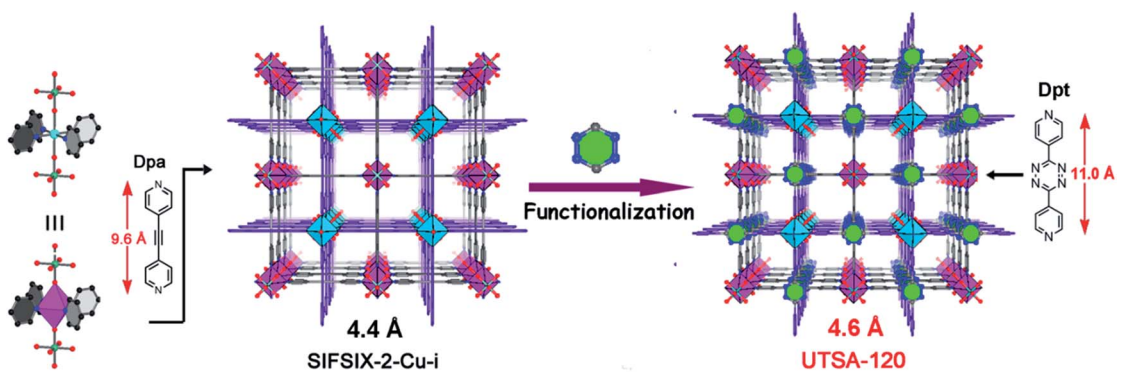

Fig. 1 Structural description of UTSA-120a, revealing its pore size (4.6 Å) and dual functionalities of SiF_6^{2-} anions and tetrazine rings around the channels. The different nets are highlighted in gray and purple for clarity. Colour code: Cu (turquoise), Si (dark green), F (red), N (blue), and C (grey).

Before evaluating UTSA-120 as a potential carbon capture adsorbent, we first examined its stability by monitoring the PXRD patterns upon sample exposure to air (Fig. 2a). When the as-synthesized sample was exposed to air for more than 6 months or to 80% humidity for 1 day, UTSA-120 could still retain its structural integrity (Fig. S3 and S4, ESI†). Even for the activated UTSA-120a sample, after exposure to air for 1 month or water vapour adsorption experiments, there is no loss of crystallinity and no obvious phase change observed (Fig. S5–S7, ESI†), indicating its excellent stability toward moisture. Next, we determined the permanent porosity of UTSA-120a using nitrogen adsorption isotherms at 77 K. As shown in Fig. S8 (ESI†) UTSA-120a can adsorb a large amount of N_2 (178 $cm^3\ g^{-1}$) at 77 K and 1 bar, and the N_2 isotherm shows a significant type I sorption behavior, characteristic of microporous materials. The Brunauer–Emmett–Teller (BET) surface area of UTSA-120a was calculated to be 638 $m^2\ g^{-1}$ (Fig. S8, ESI†), comparable to that of SIFSIX-2-Cu-i (735 $m^2\ g^{-1}$).

Next, we examined the single-component adsorption isotherms of CO_2, CH_4, and N_2 at 296 K up to 1 bar. As presented in Fig. 2a, UTSA-120a exhibits a rapid and high CO_2 uptake of 5.0 mmol g^{-1} at 296 K and 1 bar. This value is comparable to the uptake of SIFSIX-2-Cu-i (5.41 mmol g^{-1}) due to their similar pore sizes. However, incorporation of functional tetrazine groups into UTSA-120a was found to enable a significantly higher CO_2 adsorption capacity than that of SIFSIX-2-Cu-i within the low-pressure region (Fig. 2b). At 0.15 bar, which is an indicator of the CO_2 capture ability of an adsorbent from the flue gas mixture, UTSA-120a exhibits a notably enhanced CO_2 uptake (3.56 mmol g^{-1}) compared to those of SIFSIX-2-Cu-i (2.11 mmol g^{-1}) and SIFSIX-14-Cu-i (1.42 mmol g^{-1}, Fig. S9, ESI†). In comparison to other top-performing materials, the CO_2 uptake of UTSA-120a at 0.15 bar is also among the highest reported for MOF materials (Fig. 2c and Table S5, ESI†),[19] outperforming most of the well-known MOFs (*i.e.*, SIFSIX-3 and UTSA-16). Conversely, UTSA-120a shows a very low CH_4 (0.93 $cm^3\ g^{-1}$) and N_2 (0.25 $cm^3\ g^{-1}$) uptake at 1 bar and 296 K (Fig. S10 and S11, ESI†). Both values are comparable to those of SIFSIX-2-Cu-i. Therefore, the incorporation of tetrazine groups into UTSA-120a can efficiently improve the CO_2 capture capacity at a low pressure of 0.15 bar, while it has no effect on CH_4 and N_2 adsorption.

Ideal adsorbed solution theory (IAST) was employed to calculate the adsorption selectivity of UTSA-120a for 15 : 85 (v/v) CO_2/N_2 and 50/50 CO_2/CH_4 gas mixtures at 296 K. As shown in Fig. 2d and S12 (ESI†), UTSA-120a exhibits an extraordinarily high selectivity of ~600 for the CO_2/N_2 mixture, and also a high CO_2/CH_4 selectivity of up to 100.

Both values are significantly higher than those observed in SIFSIX-2-Cu-i (140 and 33 for CO_2/N_2 and CO_2/CH_4). We note that the CO_2/N_2 selectivity of UTSA-120a is only lower than those of ultra-microporous MOFs that show molecular sieving for CO_2/N_2, such as Qc-5-Cu-sql and SIFSIX-3. However, the extremely small pore spaces in those MOFs limit the CO_2

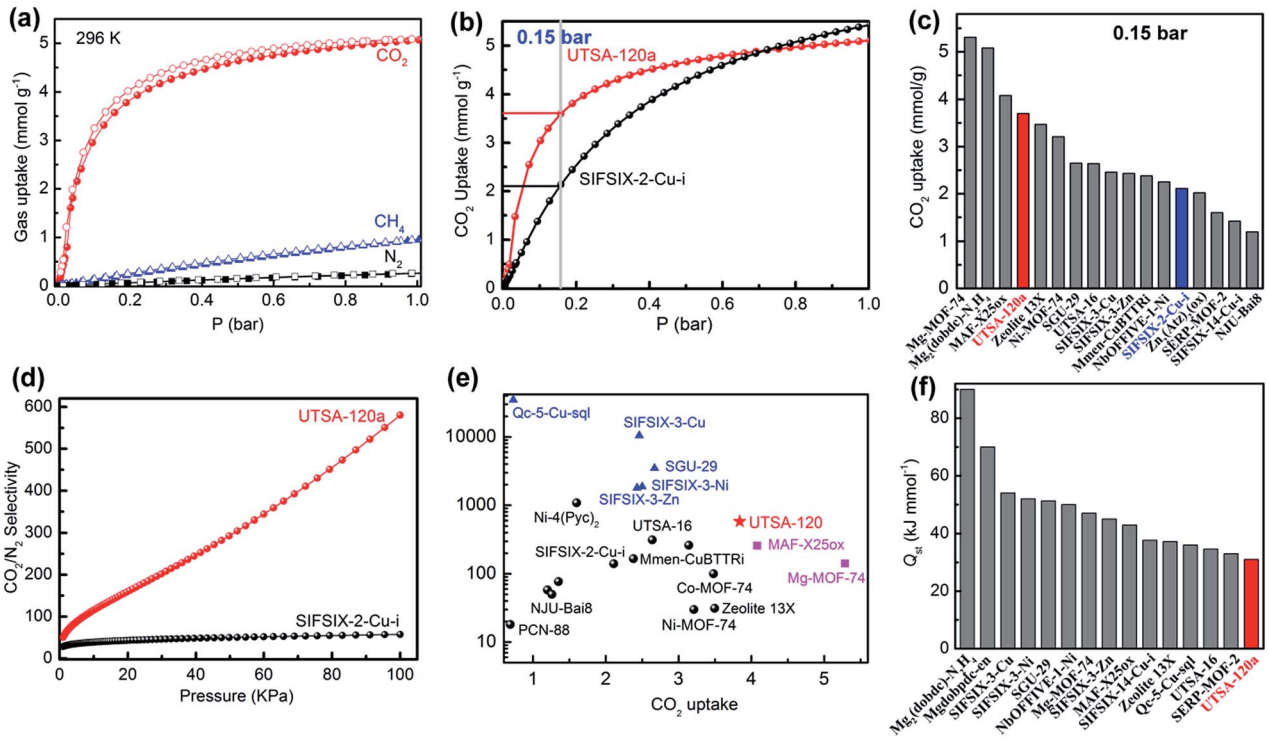

Fig. 2 (a) Gas adsorption isotherms of UTSA-120a for CO_2, CH_4 and N_2 at 296 K. Filled/empty symbols represent adsorption/desorption. (b) Comparison of CO_2 adsorption isotherms for UTSA-120a and SIFSIX-2-Cu-i at 296 K. (c) Comparison of CO_2 capture capacity for UTSA-120a and other best-performing materials at 0.15 bar and room temperature. (d) IAST selectivity of UTSA-120a (red) for CO_2/N_2 (15/85, v/v) at 296 K, as compared with SIFSIX-2-Cu-i (black). (e) A comparison of the CO_2 uptake (at 0.15 bar) and CO_2/N_2 selectivity at 1.0 bar and room temperature for UTSA-120a and other indicated MOFs. (f) Comparison of heat of CO_2 adsorption for UTSA-120a and other best-performing materials.

capture uptake at 0.15 bar, as revealed in Fig. 2e. On the other hand, although Mg-MOF-74 has the highest CO_2 capture capacity at 0.15 bar, its selectivity is relatively low (below 150). Evidently, UTSA-120a and MAF-X25ox[20] exhibit a notable balance of both high CO_2 uptake (at 0.15 bar) and high selectivity among the indicated MOFs. In addition, UTSA-120a shows the lowest Q_{st} value among the benchmark MOFs (Fig. 2f and S14, ESI†) because of its suitable pore size (~4.6 Å) and the absence of ultra-strong binding sites. Therefore, this material exhibits a rare combination of exceptional CO_2 adsorption capacity, high CO_2/N_2 selectivity and moderate Q_{st}, presumably offering a lower energy input for regeneration.

To gain better insight into the enhanced CO_2 adsorption capacity at the low-pressure region and to determine CO_2 binding sites, neutron powder diffraction data were collected on a CO_2-loaded sample of UTSA-120a and Rietveld structural refinement was conducted (see Table S7 and Fig. S2 for detailed structural information of UTSA-120a·2.6CO_2, ESI†). As shown in Fig. 3a, the adsorbed CO_2 molecules were located within the square-shaped channels of UTSA-120a, and the carbon atom of each adsorbed CO_2 molecule interacts with one SiF_6^{2-} anion through the C···F bonding with a distance of 2.741 Å. This kind of binding site has also been determined in SIFSIX-2-Cu-i.[4b] Unlike SIFSIX-2-Cu-i, we found that the carbon atom of each adsorbed CO_2 molecule also has a weaker interaction with uncoordinated N sites on tetrazine rings through the C···N bonding (3.701 Å). Additionally, the interpenetrated nature of the framework allows the SiF_6^{2-} pillars and tetrazine rings to be densely arranged around the pore channel, which creates a confined pore space to organize the CO_2 molecules densely packed along the channels with a distance of 4.553 Å (Fig. 3b). Therefore, the exceptional CO_2 uptake capacity of UTSA-120a is mainly attributed to the synergistic effect of the suitable pore size and dual functionalities that enables the optimal packing of CO_2 molecules within the pores.

Transient breakthrough simulations were performed for UTSA-120a in a fixed-bed to validate the feasibility of separation of the CO_2/N_2 (15/85) mixture that mimics the fuel gas. Fig. 3c reveals the molar concentrations of CO_2/N_2 exiting the adsorber packed with UTSA-120a as a function of dimensionless time, τ, at 1 bar and 296 K. Efficient separation was realized by UTSA-120a, whereby N_2 eluted through the bed first, and then CO_2 breakthrough occurs through the fixed-bed after a certain time (τ_{break}). Attributed to both higher selectivity and CO_2 uptake capacity, the τ_{break} value of UTSA-120a is two times longer than that observed in SIFSIX-2-Cu-i (Fig. S17, ESI†). Similarly, Fig. 3d presents that UTSA-120a can also efficiently capture CO_2 from the 50/50 CO_2/CH_4 mixture.

Experimental breakthrough studies were further conducted in a packed column of activated UTSA-120a under flow (2.0 mL min^{-1}) of binary CO_2/N_2 (15/85) and CO_2/CH_4 (50/50) mixtures at room temperature, respectively. As illustrated in Fig. 3e and f, highly efficient separation for CO_2/N_2 and CO_2/CH_4 mixtures can be accomplished by UTSA-120a. N_2 or CH_4 pass through the sample bed rapidly, while CO_2 breakthrough occurs at 84 and 36 min g^{-1} for CO_2/N_2 and CO_2/CH_4 mixtures,

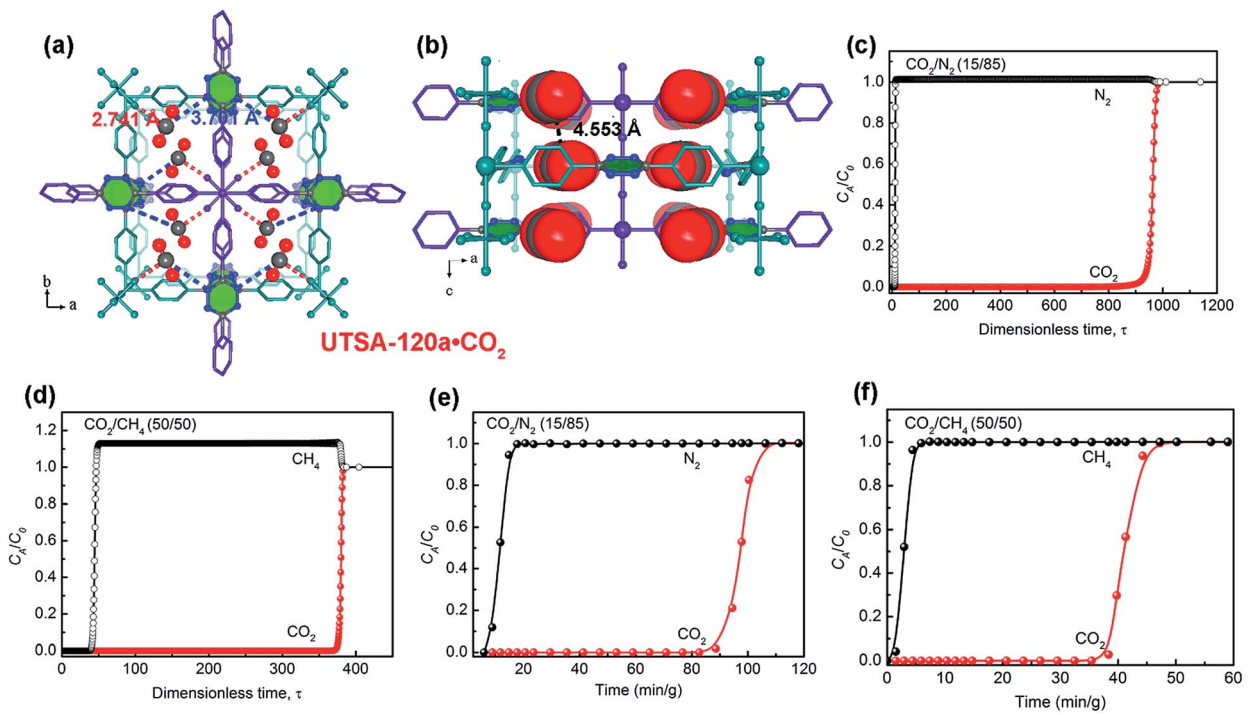

Fig. 3 (a) Neutron crystal structure of UTSA-120a·CO_2 viewed along the *c* and (b) *b* axis, determined from the Rietveld analysis (the different nets are highlighted in purple and dark green for clarity). Color code: O, red; C (in CO_2) grey. (c) Simulated column breakthrough curves for 15/85 CO_2/N_2 separation with respect to the activated UTSA-120a. (d) Simulated column breakthrough curves for CO_2/CH_4 (50/50) separation. (e) Experimental column breakthrough curves for 15/85 CO_2/N_2 and (f) 50/50 CO_2/CH_4 gas mixtures (at 298 K, 1.0 bar) with a total flow of 2 mL min^{-1} in an absorber bed packed with UTSA-120a.

respectively. These experimental breakthrough times have the same trend as the simulated breakthrough results (850 and 370 for CO_2/N_2 and CO_2/CH_4 mixtures, respectively), indicating its excellent separation performance for CO_2 capture. The adsorption bed can be easily regenerated by He flow (20 mL min^{-1}) for 15 min at 298 K, and the separation properties of UTSA-120a can be recycled several times (Fig. S18, ESI†). As inferred from the PXRD performed on the associated samples, the framework of UTSA-120a remains stable after multiple adsorption and breakthrough experiments (Fig. S19, ESI†). It should be noted that moisture would affect gas adsorption and separation performance of porous materials under humid conditions.[21] To further confirm the moisture stability of UTSA-120a, we measured the CO_2 adsorption properties of UTSA-120a after exposure of the sample to air for 1 month. The results revealed that the re-activated sample retains its CO_2 adsorption capacity (Fig. S20, ESI†).

Conclusions

In summary, we designed and synthesized a novel SIFSIX material (UTSA-120a) by using a functionalized organic linker of dpt instead of dpa in SIFSIX-2-Cu-i. The foregoing results revealed that UTSA-120a exhibits very high CO_2 capture capacity (3.56 mmol g^{-1} at 0.15 bar and 296 K) and exceptional separation selectivity (~600). Both values outperform those of the isoreticular SIFSIX-2-Cu-i and most of the other reported MOFs. This exceptional separation performance is mainly attributed to the suitable pore size and dual functionalities on pore surfaces to not only interact with CO_2 molecules but also enable the dense packing of CO_2 molecules within the pores, as revealed by the UTSA-120a·2.6CO_2 structure. The rare combination of very high CO_2 adsorption capacity, exceptional CO_2/N_2 selectivity, and moderate heat of CO_2 adsorption renders UTSA-120a a very promising candidate for CO_2 capture from flue gases. Breakthrough experiments confirmed that UTSA-120a can efficiently capture CO_2 gas from the CO_2/N_2 and CO_2/CH_4 mixtures.

Experimental section

Synthesis of $[Cu(dpt)_2(SiF_6)]_n$ (UTSA-120)

60 mg (0.25 mmol) of 3,6-di(4-pyridyl)-1,2,4,5-tetrazine (dpt) was partially dissolved in a methanol solution (30 mL). An aqueous solution of $CuSiF_6$ (1.0 mL, 0.247 mmol) was then added dropwise to the stirred methanol solution. A fresh pink precipitate appeared immediately, and the solution was then stirred for 24 hours at room temperature. The suspension was filtered, and the precipitate was washed with MeOH and then air dried. Bulk purity of the sample was verified by PXRD (Fig. S1, ESI†).

Gas sorption measurements

Gas adsorption isotherms were measured using a MicromeriticsASAP 2020 surface area analyzer. To remove all the guest solvents in the framework, the fresh powder sample was first solvent-exchanged with dry methanol at least 8 times within two days. The solvent-exchanged sample was evacuated at room temperature for 24 h, at 323 K for 12 h and then at 343 K for an additional 4–5 h till the outgas rate was 5 mmHg min^{-1} prior to measurements. The sorption measurement was maintained at 77 K with liquid nitrogen. An ice-water bath (slush) and water bath were used for adsorption isotherms at 273 and 296 K, respectively.

Neutron diffraction experiment

High-resolution neutron diffraction data were collected using a BT-1 neutron powder diffractometer at the National Institute of Standards and Technology (NIST) Center for Neutron Research. A Ge(311) monochromator with a 75° take-off angle, $\lambda = 2.0787(2)$ Å, and in-pile collimation of 60 minutes of arc was used. Data were collected over the range of 1.3–166.3° (2θ) with a step size of 0.05°. The fully activated UTSA-120a sample was loaded in a vanadium can equipped with a capillary gas line and a packless valve. A closed-cycle He refrigerator was used for sample temperature control. The bare MOF sample was measured first, at room temperature (296 K). To probe the CO_2 adsorption location, a pre-determined amount of CO_2 was loaded into the sample at room temperature, and diffraction data were then collected. Rietveld structural refinement was performed on the neutron diffraction data using the GSAS package.[22] The refinements on lattice parameters, atomic coordinates, positions/orientations of the CO_2 molecules (treated as rigid bodies), CO_2 occupancies, thermal factors, background, and profiles all converge with satisfactory *R*-factors. The structural data are summarized in Table S7.†

Breakthrough experiments

The breakthrough curves were measured on a homemade apparatus for gas mixtures CO_2/N_2 (15/85) or CO_2/CH_4 (50/50) at 298 K and 1.01 bar. In the separation experiment, the activated UTSA-120a (0.582 g) particles with diameters of 200–300 μm were prepared and packed into a Φ 4 × 150 mm stainless steel column. The experimental set-up consisted of two fixed-bed stainless steel reactors. One reactor was loaded with the adsorbent, while the other reactor was used as a blank control group to stabilize the gas flow. The gas flows were controlled at the inlet using a mass flow meter at 2 mL min^{-1}, and a gas chromatograph (TCD – Thermal Conductivity Detector, detection limit 0.1 ppm) continuously monitored the effluent gas from the adsorption bed. Prior to every breakthrough experiment, we activated the sample by flushing the adsorption bed with helium gas for 2 hours at 323 K. Subsequently, the column was allowed to equilibrate at the measurement rate before we switched the gas flow. The adsorption bed was easily regenerated by He flow (20 mL min^{-1}) for 15 min at 298 K.

Conflicts of interest

There are no conflicts to declare.

Acknowledgements

This work was supported by an award AX-1730 from the Welch Foundation (BC), the National Natural Science Foundation of China (51672248 and 51872261), the Zhejiang Provincial Natural Science Foundation of China (No. LY19B010004 and LR19E020002), and the Qianjiang Talent plan of Zhejiang Province (QJD1802018). The Distinguished Scientist Fellowship Program (DSFP) at KSU is gratefully acknowledged for supporting this work.

Notes and references

1 K. Feng, S. J. Davis, L. Sun and K. Hubacek, *Nat. Commun.*, 2015, **6**, 7714.

2 S. Chu, Y. Cui and N. Liu, *Nat. Mater.*, 2017, **16**, 16.

3 A. Schoedel, Z. Ji and O. M. Yaghi, *Nat. Energy*, 2016, **1**, 16034.

4 (*a*) M. T. Ho, G. W. Allinson and D. E. Wiley, *Ind. Eng. Chem. Res.*, 2008, **47**, 4883; (*b*) P. Nugent, Y. Belmabkhout, S. D. Burd, A. J. Cairns, R. Luebke, K. Forrest, T. Pham, S. Ma, B. Space, L. Wojtaset, M. Eddaoudi and M. J. Zaworotko, *Nature*, 2013, **495**, 80.

5 (*a*) H. Furukawa, K. E. Cordova, M. O'Keeffe and O. M. Yaghi, *Science*, 2013, **341**, 6149; (*b*) B. Li, H.-M. Wen, Y. Cui, W. Zhou, G. Qian and B. Chen, *Adv. Mater.*, 2016, **28**, 8819; (*c*) S. Furukawa, J. Reboul, S. Diring, K. Sumida and S. Kitagawa, *Chem. Soc. Rev.*, 2014, **43**, 5700.

6 (*a*) P. Li, N. A. Vermeulen, C. D. Malliakas, D. A. Gómez-Gualdrón, A. J. Howarth, B. L. Mehdi, A. Dohnalkova, N. D. Browning, M. O'Keeffe and O. K. Farha, *Science*, 2017, **356**, 624; (*b*) B. Li, M. Chrzanowski, Y. Zhang and S. Ma, *Coord. Chem. Rev.*, 2016, **307**, 106; (*c*) H. Wang, X. Dong, V. Colombo, Q. Wang, Y. Liu, W. Liu, X.-L. Wang, X.-Y. Huang, D. M. Proserpio, A. Sironi, Y. Han and J. Li, *Adv. Mater.*, 2018, **30**, 1805088.

7 (*a*) C. A. Trickett, A. Helal, B. A. Al-Maythalony, Z. H. Yamani, K. E. Cordova and O. M. Yaghi, *Nat. Rev. Mater.*, 2017, **2**, 17045; (*b*) J. Yu, L.-H. Xie, J.-R. Li, Y. Ma, J. M. Seminario and P. B. Balbuena, *Chem. Rev.*, 2017, **117**, 9674; (*c*) K. Sumida, D. L. Rogow, J. A. Mason, T. M. McDonald, E. D. Bloch, Z. R. Herm, T.-H. Bae and J. R. Long, *Chem. Rev.*, 2012, **112**, 724; (*d*) Z. Zhang, Z.-Z. Yao, S. Xiang and B. Chen, *Energy Environ. Sci.*, 2014, **7**, 2868; (*e*) B. Li, H.-M. Wen, Y. Yu, Y. Cui, W. Zhou, B. Chen and G. Qian, *Mater. Today Nano*, 2018, **2**, 21.

8 (*a*) S. R. Caskey, A. G. Wong-Foy and A. J. Matzger, *J. Am. Chem. Soc.*, 2008, **130**, 10870; (*b*) A. Ö. Yazaydın, R. Q. Snurr, T.-H. Park, K. Koh, J. Liu, M. D. LeVan, A. I. Benin, P. Jakubczak, M. Lanuza, D. B. Galloway, J. J. Low and R. R. Willis, *J. Am. Chem. Soc.*, 2009, **131**, 18198; (*c*) D. Britt, H. Furukawa, B. Wang, T. G. Glover and O. M. Yaghi, *Proc. Natl. Acad. Sci. U. S. A.*, 2009, **106**, 20637.

9 (*a*) L. Hamon, P. L. Llewellyn, T. Devic, A. Ghoufi, G. Clet, V. Guillerm, G. D. Pirngruber, G. Maurin, C. Serre, G. Driver, W. Beek, E. Jolimaître, A. Vimont, M. Daturi and G. Férey, *J. Am. Chem. Soc.*, 2009, **131**, 17490; (*b*) H.-S. Choi and M. P. Suh, *Angew. Chem., Int. Ed.*, 2009, **48**, 6865; (*c*) Z. Chang, D.-H. Yang, J. Xu, T.-L. Hu and X.-H. Bu, *Adv. Mater.*, 2015, **27**, 5432.

10 (*a*) B. Zheng, J. Bai, J. Duan, L. Wojtas and M. J. Zaworotko, *J. Am. Chem. Soc.*, 2011, **133**, 748; (*b*) H. Wang, X. Dong, J. Lin, S. J. Teat, S. Jensen, J. Cure, E. V. Alexandrov, Q. Xia, K. Tan, Q. Wang, D. H. Olson, D. M. Proserpio, Y. J. Chabal, T. Thonhauser, J. Sun, Y. Han and J. Li, *Nat. Commun.*, 2018, **9**, 1745; (*c*) J.-B. Lin, J.-P. Zhang and X.-M. Chen, *J. Am. Chem. Soc.*, 2010, **132**, 6654; (*d*) J. An, S. J. Geib and N. L. Rosi, *J. Am. Chem. Soc.*, 2010, **132**, 38; (*e*) Y. Yuan, P. Cui, Y. Tian, X. Zou, Y. Zhou, F. Sun and G. Zhu, *Chem. Sci.*, 2016, **7**, 3751; (*f*) H.-R. Fu and J. Zhang, *Chem.–Eur. J.*, 2015, **21**, 5700.

11 (*a*) Q.-G. Zhai, X. Bu, C. Mao, X. Zhao, L. Daemen, Y. Cheng, A. J. Ramirez-Cuesta and P. Feng, *Nat. Commun.*, 2016, **7**, 13645; (*b*) Z. Niu, S. Fang, X. Liu, J. G. Ma, S. Ma and P. Cheng, *J. Am. Chem. Soc.*, 2015, **137**, 14873; (*c*) L. Du, Z. Lu, K. Zheng, J. Wang, X. Zheng, Y. Pan, X. You and J. Bai, *J. Am. Chem. Soc.*, 2013, **135**, 562; (*d*) J.-R. Li, J. Yu, W. Lu, L.-B. Sun, J. Sculley, P. B. Balbuena and H.-C. Zhou, *Nat. Commun.*, 2013, **4**, 1538; (*e*) N. Ding, H. Li, X. Feng, Q. Wang, S. Wang, L. Ma, J. Zhou and B. Wang, *J. Am. Chem. Soc.*, 2016, **138**, 10100; (*f*) S. Nandi, S. Collins, D. Chakraborty, D. Banerjee, P. K. Thallapally, T. K. Woo and R. Vaidhyanathan, *J. Am. Chem. Soc.*, 2017, **139**, 1734; (*g*) Z. G. Hu, Y. X. Wang, S. Farooq and D. Zhao, *AIChE J.*, 2017, **63**, 4103.

12 (*a*) S. Xiang, Y. He, Z. Zhang, H. Wu, W. Zhou, R. Krishna and B. Chen, *Nat. Commun.*, 2012, **3**, 954; (*b*) R. W. Flaig, T. M. Osborn Popp, A. M. Fracaroli, E. A. Kapustin, M. J. Kalmutzki, R. M. Altamimi, F. Fathieh, J. A. Reimer and O. M. Yaghi, *J. Am. Chem. Soc.*, 2017, **139**, 12125; (*c*) Z. Lu, H. G. W. Godfrey, I. d. Silva, Y. Cheng, M. Savage, F. Tuna, E. J. L. McInnes, S. J. Teat, K. J. Gagnon, M. D. Frogley, P. Manuel, S. Rudić, A. J. Ramirez-Cuesta, T. L. Easun, S. Yang and M. Schröder, *Nat. Commun.*, 2017, **8**, 14212; (*d*) L. Liang, C. Liu, F. Jiang, Q. Chen, L. Zhang, H. Xue, H.-L. Jiang, J. Qian, D. Yuan and M. Hong, *Nat. Commun.*, 2017, **8**, 1233; (*e*) Z.-J. Lin, Y.-B. Huang, T.-F. Liu, X.-Y. Li and R. Cao, *Inorg. Chem.*, 2013, **52**, 3127; (*f*) X. Lv, L. Li, S. Tang, C. Wang and X. Zhao, *Chem. Commun.*, 2014, **50**, 6886.

13 (*a*) O. Shekhah, Y. Belmabkhout, Z. Chen, V. Guillerm, A. Cairns, K. Adil and M. Eddaoudi, *Nat. Commun.*, 2014, **5**, 4228; (*b*) H.-M. Wen, L. Li, R.-B. Lin, B. Li, B. Hu, W. Zhou, J. Hu and B. Chen, *J. Mater. Chem. A*, 2018, **6**, 6931; (*c*) S. K. Elsaidi, M. H. Mohamed, H. T. Schaef, A. Kumar, M. Lusi, T. Pham, K. A. Forrest, B. Space, W. Xu, G. J. Halder, J. Liu, M. J. Zaworotko and P. K. Thallapally, *Chem. Commun.*, 2015, **51**, 15530; (*d*) P. M. Bhatt, Y. Belmabkhout, A. Cadiau, K. Adil, O. Shekhah, A. Shkurenko, L. J. Barbour and M. Eddaoudi, *J. Am. Chem. Soc.*, 2016, **138**, 9301.

14 (*a*) K.-J. Chen, D. G. Madden, T. Pham, K. A. Forrest, A. Kumar, Q.-Y. Yang, W. Xue, B. Space, J. J. Perry IV, J.-P. Zhang, X.-M. Chen and M. J. Zaworotko, *Angew. Chem., Int. Ed.*, 2016, **55**, 10268; (*b*) M. Du, C.-P. Li,

M. Chen, Z.-W. Ge, X. Wang, L. Wang and C.-S. Liu, *J. Am. Chem. Soc.*, 2014, **136**, 10906.

15 (*a*) P.-Q. Liao, X.-W. Chen, S.-Y. Liu, X.-Y. Li, Y.-T. Xu, M. Tang, Z. Rui, H. Ji, J.-P. Zhang and X.-M. Chen, *Chem. Sci.*, 2016, **7**, 6528; (*b*) A. Demessence, D. M. D'Alessandro, M. L. Foo and J. R. Long, *J. Am. Chem. Soc.*, 2009, **131**, 8784; (*c*) T. M. McDonald, D. M. D'Alessandro, R. Krishna and J. R. Long, *Chem. Sci.*, 2011, **2**, 2022; (*d*) T. M. McDonald, J. A. Mason, X. Kong, E. D. Bloch, D. Gygi, A. Dani, V. Crocellá, F. Giordanino, S. O. Odoh, W. S. Drisdell, B. Vlaisavljevich, A. L. Dzubak, R. Poloni, S. K. Schnell, N. Planas, K. Lee, T. Pascal, L. F. Wan, D. Prendergast, J. B. Neaton, B. Smit, J. B. Kortright, L. Gagliardi, S. Bordiga, J. A. Reimer and J. R. Long, *Nature*, 2015, **519**, 303.

16 (*a*) S. Subramanian and M. J. Zaworotko, *Angew. Chem., Int. Ed.*, 1995, **34**, 2127; (*b*) S. D. Burd, S. Ma, J. A. Perman, B. J. Sikora, R. Q. Snurr, P. K. Thallapally, J. Tian, L. Wojtas and M. J. Zaworotko, *J. Am. Chem. Soc.*, 2012, **134**, 3663; (*c*) X. Cui, K. Chen, H. Xing, Q. Yang, R. Krishna, Z. Bao, H. Wu, W. Zhou, X. Dong, Y. Han, B. Li, Q. Ren, M. J. Zaworotko and B. Chen, *Science*, 2016, **353**, 141.

17 (*a*) L. Li, R.-B. Lin, R. Krishna, H. Li, S. Xiang, H. Wu, J. Li, W. Zhou and B. Chen, *Science*, 2018, **362**, 443; (*b*) R.-B. Lin, L. Li, H.-L. Zhou, H. Wu, C. He, S. Li, R. Krishna, J. Li, W. Zhou and B. Chen, *Nat. Mater.*, 2018, **17**, 1128; (*c*) G. Xu, B. Li, H. Wu, W. Zhou and B. Chen, *Cryst. Growth Des.*, 2017, **17**, 4795.

18 (*a*) J. P. Zhang and X. M. Chen, *J. Am. Chem. Soc.*, 2009, **131**, 5516; (*b*) S.-J. Bao, R. Krishna, Y.-B. He, J.-S. Qin, Z.-M. Su, S.-L. Li, W. Xie, D.-Y. Du, W.-W. He, S.-R. Zhang and Y.-Q. Lan, *J. Mater. Chem. A*, 2015, **3**, 7361; (*c*) B. Li, Z. Zhang, Y. Li, K. Yao, Y. Zhu, Z. Deng, F. Yang, X. Zhou, G. Li, H. Wu, N. Nijem, Y. J. Chabal, Z. Lai, Y. Han, Z. Shi, S. Feng and J. Li, *Angew. Chem., Int. Ed.*, 2012, **51**, 1412; (*d*) C. Song, J. Hu, Y. Ling, Y. Feng, R. Krishna, D.-l. Chen and Y. He, *J. Mater. Chem. A*, 2015, **3**, 19417.

19 (*a*) S. J. Datta, C. Khumnoon, Z. H. Lee, W. K. Moon, S. Docao, T. H. Nguyen, I. C. Hwang, D. Moon, P. Oleynikov, O. Terasaki and K. B. Yoon, *Science*, 2015, **350**, 302; (*b*) A. Kumar, D. G. Madden, M. Lusi, K.-J. Chen, E. A. Daniels, T. Curtin, J. J. Perry IV and M. J. Zaworotko, *Angew. Chem., Int. Ed.*, 2015, **54**, 14372; (*c*) R. Vaidhyanathan, S. S. Iremonger, G. K. H. Shimizu, P. G. Boyd, S. Alavi and T. K. Woo, *Science*, 2010, **330**, 650.

20 P.-Q. Liao, H. Chen, D.-D. Zhou, S.-Y. Liu, C.-T. He, Z. Rui, H. Ji, J.-P. Zhang and X.-M. Chen, *Energy Environ. Sci.*, 2015, **8**, 1011.

21 (*a*) J. A. Mason, T. M. McDonald, T.-H. Bae, J. E. Bachman, K. Sumida, J. J. Dutton, S. S. Kaye and J. R. Long, *J. Am. Chem. Soc.*, 2015, **137**, 4787; (*b*) D. O'Nolan, A. Kumar and M. J. Zaworotko, *J. Am. Chem. Soc.*, 2017, **139**, 8508; (*c*) D. G. Madden, H. S. Scott, A. Kumar, K.-J. Chen, R. Sanii, A. Bajpai, M. Lusi, T. Curtin, J. J. Perry and M. J. Zaworotko, *Philos. Trans. R. Soc., A*, 2017, **375**, 20160025.

22 A. C. Larson and R. B. V. Dreele, *General Structure Analysis System, LAUR 86-748*, Los Alamos National Laboratory, 1994.

Supporting Information

A metal−organic framework with suitable pore size and dual functionalities for highly efficient post-combustion CO_2 capture

Hui-Min Wen[a], Caijun Liao[a], Libo Li[b,c], Ali Alsalme[d], Zeid Alothman[d], Rajamani Krishna[e], Hui Wu[f], Wei Zhou[f]*, Jun Hu[a]* and Banglin Chen[b]*

[a] College of Chemical Engineering, Zhejiang University of Technology, Zhejiang, 310014, China. E-mail: hjzjut@zjut.edu.cn

[b] Department of Chemistry, University of Texas at San Antonio, One UTSA Circle, San Antonio, Texas 78249-0698, USA. Fax: (+1)-210-458-7428. E-mail: banglin.chen@utsa.edu

[c] College of Chemistry and Chemical Engineering, Taiyuan University of Technology, Taiyuan 030024, Shanxi, China

[d] Chemistry Department, College of Science, King Saud University, P O Box 2455, Riyadh 11451, Saudi Arabia

[e] Van't Hoff Institute for Molecular Sciences, University of Amsterdam, Science Park 904, 1098 XH Amsterdam, Netherlands

[f] NIST Center for Neutron Research, National Institute of Standards and Technology, Gaithersburg, MD 20899-6102, USA. E-mail: wzhou@nist.gov

1. General Procedures and Materials. All starting reagents and solvents were purchased from commercial companies and used without further purification. Powder X–ray diffraction (PXRD) patterns were performed by a Rigaku Ultima IV diffractometer operated at 40 kV and 44 mA with a scan rate of 2.0 deg min^{-1}.

2. Fitting of pure component isotherms

The experimentally measured loadings for CO_2 measured at temperatures of 273 K, and 296 K in UTSA-120 and SIF-SIX-2-Cu-i were fitted with the dual-Langmuir-Freundlich isotherm model

$$q = q_{A,sat}\frac{b_A p^{\nu_A}}{1+b_A p^{\nu_A}} + q_{B,sat}\frac{b_B p^{\nu_B}}{1+b_B p^{\nu_B}} \tag{1}$$

with T-dependent parameters b_A, and b_B

$$b_A = b_{A0}\exp\left(\frac{E_A}{RT}\right); \quad b_B = b_{B0}\exp\left(\frac{E_B}{RT}\right) \tag{2}$$

The parameters are provided in Table S2.

The isotherm data for CH_4, and N_2 measured at temperatures of 273 K, and 296 K in UTSA-120 and SIF-SIX-2-Cu-i were fitted with good accuracy with the single-site Langmuir model

$$q = q_{sat}\frac{bp}{1+bp} \tag{3}$$

with T-dependent parameters

$$b = b_0\exp\left(\frac{E}{RT}\right) \tag{4}$$

The parameters are provided in Table S3, and Table S4.

3. Virial Graph Analysis

Estimation of the isosteric heats of gas adsorption (Q_{st})

A virial-type expression of comprising the temperature-independent parameters a_i and b_j was employed to calculate the enthalpies of adsorption for CO_2 (at 273 K and 296 K) on UTSA-120a. In each case, the data were fitted use equation:

$$\ln P = \ln N + 1/T \sum_{i=0}^{m} a_i N_i + \sum_{j=0}^{n} b_j N_j \quad (5)$$

Here, P is the pressure expressed in Pa, N is the amount absorbed in mmol g^{-1}, T is the temperature in K, a_i and b_j are virial coefficients, and m, n represent the number of coefficients required to adequately describe the isotherms (m and n were gradually increased till the contribution of extra added a and b coefficients was deemed to be statistically insignificant towards the overall fit. And the average value of the squared deviations from the experimental values was minimized). The values of the virial coefficients a_0 through a_m were then used to calculate the isosteric heat of absorption using the following expression:

$$Q_{st} = -R \sum_{i=0}^{m} a_i N_i \quad (6)$$

Q_{st} is the coverage-dependent isosteric heat of adsorption and R is the universal gas constant. The heat enthalpy of CO_2 sorption for complex UTSA-120a in this manuscript are determined by using the sorption data measured in the pressure range from 0-1 bar (at 273 K and 296 K).

4. IAST calculations

The adsorption selectivity is defined by

$$S_{ads} = \frac{q_1/q_2}{p_1/p_2} \quad (7)$$

In equation (7), q_1, and q_2 are the molar loadings in the adsorbed phase in equilibrium with the bulk gas phase with partial pressures p_1, and p_2.

Figure 2d presents IAST calculations for binary 15/85 CO_2/N_2 mixtures at 296 K. The CO_2 uptake is significantly higher in UTSA-120a as compared to SIF-SIX-2-Cu-i. The CO_2/N_2 selectivity is about an order of magnitude higher in UTSA-120a as compared to SIF-SIX-2-Cu-i.

Figure S12 presents IAST calculations for 50/50 CO_2/CH_4 mixtures at 296 K. Also in this case the separations are better in UTSA-120a as compared to SIF-SIX-2-Cu-i.

5. Transient breakthrough of mixtures in fixed bed adsorbers

The performance of industrial fixed bed adsorbers is dictated by a combination of adsorption selectivity and uptake capacity. For a proper comparison of various MOFs, we perform transient

breakthrough simulations using the simulation methodology described in the literature.[1,2] For the breakthrough simulations, the following parameter values were used: length of packed bed, L = 0.3 m; voidage of packed bed, ε = 0.4; superficial gas velocity at inlet, u = 0.04 m/s. The transient breakthrough simulation results are presented in terms of a *dimensionless* time, τ, defined by dividing the actual time, t, by the characteristic time, $\frac{L\varepsilon}{u}$.

Notation

b_A	Langmuir-Freundlich constant for species *i* at adsorption site A, $Pa^{-\nu_{iA}}$
b_B	Langmuir-Freundlich constant for species *i* at adsorption site B, $Pa^{-\nu_{iB}}$
c_i	molar concentration of species *i* in gas mixture, mol m^{-3}
c_{i0}	molar concentration of species *i* in gas mixture at inlet to adsorber, mol m^{-3}
E	energy parameter, J mol^{-1}
L	length of packed bed adsorber, m
p_i	partial pressure of species *i* in mixture, Pa
p_t	total system pressure, Pa
q_i	component molar loading of species *i*, mol kg^{-1}
Q_{st}	isosteric heat of adsorption, J mol^{-1}
t	time, s
T	absolute temperature, K
u	superficial gas velocity in packed bed, m s^{-1}

Greek letters

ε	voidage of packed bed, dimensionless
ν	Freundlich exponent, dimensionless
ρ	framework density, kg m^{-3}
τ	time, dimensionless

Subscripts

i	referring to component *i*
t	referring to total mixture

Table S1. The structural details for fully activated UTSA-120a, obtained from Rietveld refinement of the neutron diffraction data.

Unit cell parameters	UTSA-120a
Formula	$C_{24}H_{16}CuF_6N_{12}Si$
Formula weight	678.10
Crystal system	Tetragonal
Space group	I4/mmm
a, b (Å)	15.123(11)
c (Å)	7.8349(1)
α (°)	90.00
β (°)	90.00
γ (°)	90.00
V (Å^3)	1791.89(34)
Z	2
D_{calcd} (g cm^{-3})	1.257
R_{wp}, R_p	0.0207, 0.0170
CCDC	1882294

Table S2. Dual-Langmuir-Freundlich parameter fits for CO_2 in UTSA-120a and SIFSIX-2-Cu-i. The fits are based on experimental isotherm data at 296 K.

	Site A				Site B			
	$q_{A,sat}$ mol kg^{-1}	b_{A0} $Pa^{-\nu A}$	E_A kJ mol^{-1}	ν_A dimensionless	$q_{B,sat}$ mol kg^{-1}	b_{B0} $Pa^{-\nu B}$	E_B kJ mol^{-1}	ν_B dimensionless
UTSA-120a	0.57	4.81×10^{-18}	26.4	2.65	4.7	2.41×10^{-11}	31.3	1.34
SIF-SIX-2-Cu-i	2.4	7.87×10^{-10}	17.6	1.1	6	6.23×10^{-12}	34.8	1..14

Table S3. Langmuir parameter fits for CH_4 in UTSA-120a and SIFSIX-2-Cu-i. The fits are based on experimental isotherm data at 296 K.

	q_{sat} mol kg^{-1}	b_0 Pa^{-1}	E kJ mol^{-1}
UTSA-120a	3.3	1.78×10^{-8}	13.3
SIF-SIX-2-Cu-i	5	9.89×10^{-8}	6.6

Table S4. Langmuir parameter fits for N_2 in UTSA-120a and SIFSIX-2-Cu-i. The fits are based on experimental isotherm data at 296 K.

	q_{sat} mol kg^{-1}	b_0 Pa^{-1}	E kJ mol^{-1}
UTSA-120	1.75	4.63×10^{-9}	14.6
SIF-SIX-2-Cu-i	4.1	1.35×10^{-7}	4.3

Table S5. Comparison of the CO_2 adsorption capacity and CO_2/N_2 selectivity of UTSA-120a with other high-performing materials at room temperature.

MOFs	Adsorption uptake		CO_2/N_2 selectivity	Q_{st} (kJ/mol)	Ref.
	0.15 bar (mmol g^{-1})	1.0 bar (mmol g^{-1})			
UTSA-120a	**3.56**	**5.0**	**600**	**27-31**	This work
Mg-MOF-74	5.31	8.04	148	47	3
$Mg_2(dobdc)(N_2H_4)_{1.8}$	5.18	5.51	-	90	4
MAF-X25ox	4.08	7.1	250	43	5
Co-MOF-74	3.48	5.53	100	37	6
Zeolite 13X	3.47	-	30.4	37.2	6
Ni-MOF-74	3.21	5.80	30	42	6
Mg-dobpdc-mmen	3.14	4.0	262	70	7
SGU-29	2.65	3.53	3515	51.3	8
UTSA-16	2.64	4.3	314	34.6	6
SIFSIX-3-Ni	2.5	2.55	1874	52	9
SIFSIX-3-Cu	2.46	2.46	10500	54	10
SIFSIX-3-Zn	2.43	2.54	1800	45	11
CuBTTRi-mmen	2.38	4.17	166	96	12
NbOFFIVE-1-Ni	2.25	2.25	-	50	13
SIFSIX-2-Cu-i	2.11	5.41	140	31.9	11
$Zn_2(Atz)_2(ox)$	2.02	3.62	-	40.8	14
SERP-MOF-2	1.6	3.08	1084	33	15
SIFSIX-14-Cu-i	1.42	4.68	-	37.7	16
Bio-MOF-11	1.35	4.05	76.8	45	17
CPM-231	1.26	6.77	50	20.4	18
NJU-Bai8	1.2	2.51	58	37.7	19
Qc-5-Cu-sql	0.73	2.16	35000	36	20
PCN-88	0.69	4.20	18.1	27	21

Table S6. Comparison of the CO_2 adsorption capacity, CO_2/CH_4 selectivity, and Q_{st} of UTSA-120a with other high-performing materials at room temperature.

MOFs	Adsorption uptake		CO_2/CH_4 selectivity	Q_{st} (kJ/mol)	Ref.
	0.15 bar (mmol g^{-1})	1.0 bar (mmol g^{-1})			
UTSA-120a	**3.56**	**5.0**	**96**	**27-31**	This work
Qc-5-Cu-sql	0.73	2.16	3300	36	20
SIFSIX-3-Zn	2.43	2.54	231	45	11
Mg-MOF-74	5.31	8.04	105	47	6
NaX	-	4.81	60	34.5	6
SIFSIX-2-Cu-i	2.11	5.41	33	31.9	11
UTSA-16	2.64	4.3	29.8	34.6	6
NJU-Bai8	1.2	2.51	15.9	37.7	19
Cu-TDPAT	1.73	5.09	13.8	42.2	22
ZIF-78	1.04	2.05	10.6	29	6
HKUST-1	1.15	5.44	7.4	35	6
Zn-MOF-74	1.83	5.32	5.0	31.7	23

Table S7. The structural details of the CO_2-loaded sample (UTSA-120a·2.6CO_2), obtained from Rietveld refinement of the neutron diffraction data.

Unit cell parameters of UTSA-200·2.6CO_2	
Formula	$C_{26.60}\,H_{16.00}\,Cu\,F_6\,N_{12.00}\,O_{5.20}\,Si$
Formula weight	792.47
Temperature/K	300
Crystal system	Tetragonal
Space group	I4/mmm
a (Å)	15.1068(7)
b (Å)	15.1068(7)
c (Å)	7.9980(8)
α (°)	90.0
β (°)	90.0
γ (°)	90.0
V (Å^3)	1825.3(4)
Z	2
R_{wp}, R_p	0.0238, 0.0198
CCDC number	1881280

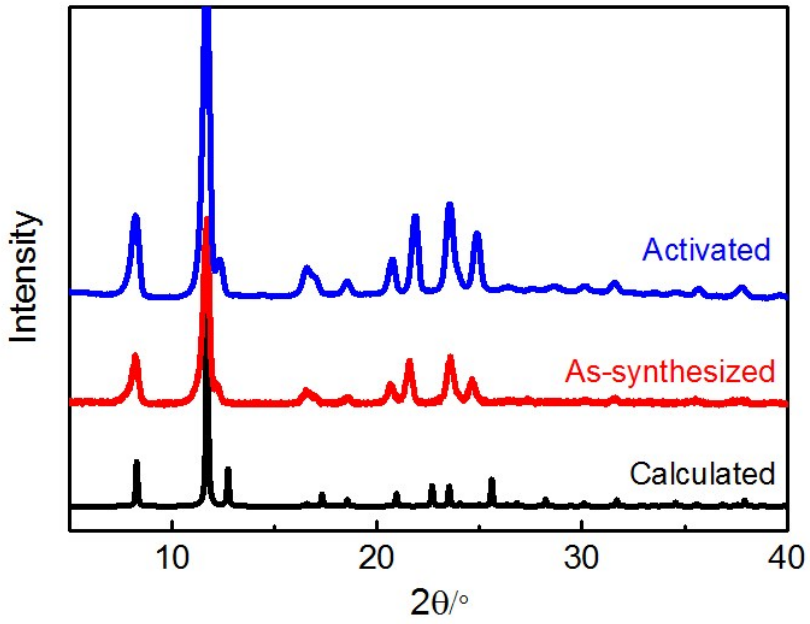

Figure S1. PXRD patterns of as-synthesized UTSA-120 (red) and activated UTSA-120a (blue) along with the calculated XRD pattern based on the neutron diffraction structure of UTSA-120a (black).

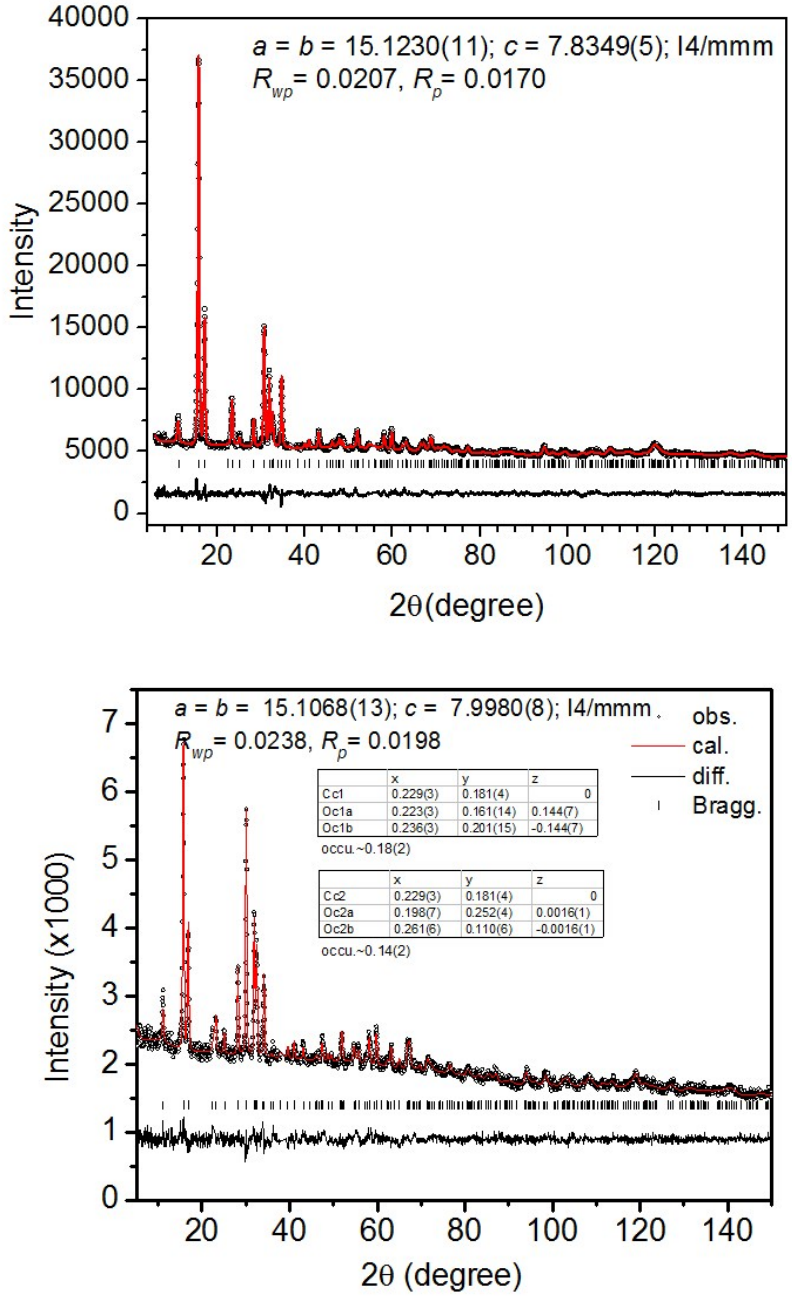

Figure S2. Rietveld refinements of the neutron powder diffraction data for bare UTSA-120a (the upper panel) and CO_2-loaded UTSA-120a (the lower panel). The goodness of fit data and the refined CO_2 locations are shown in inset.

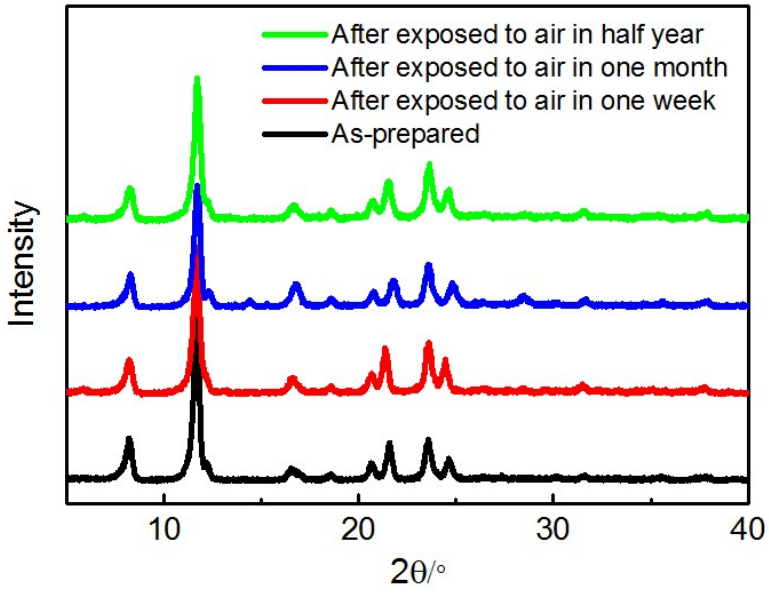

Figure S3. Experimental PXRD patterns of as-synthesized UTSA-120 sample and the sample after exposure to the air for one week, one month and half year, respectively, indicating its good stability toward moisture.

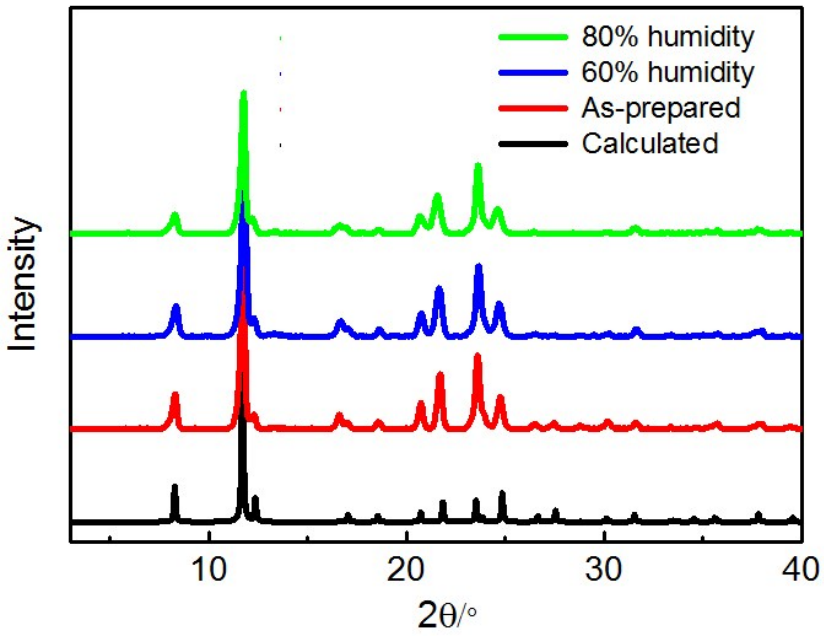

Figure S4. Experimental PXRD patterns of as-synthesized UTSA-120 sample and the sample exposed to variable humidity levels for one day.

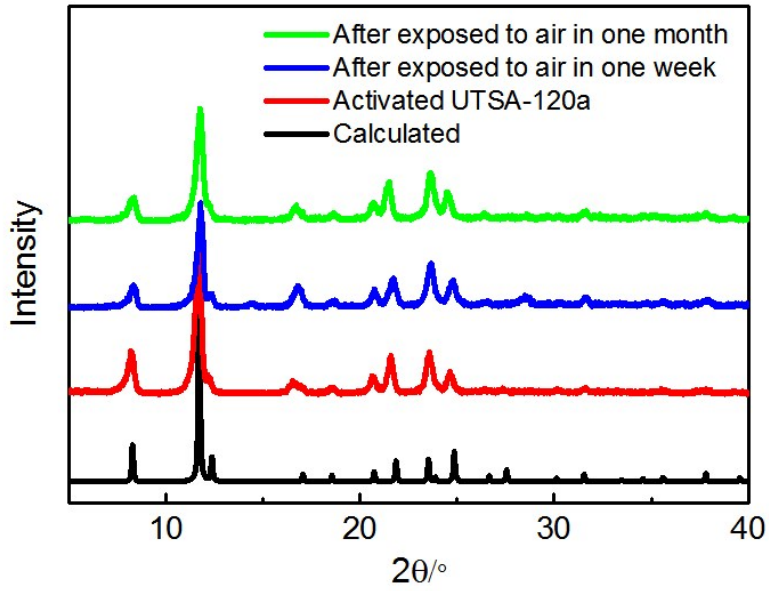

Figure S5. Experimental PXRD patterns of the activated UTSA-120a sample and the sample after exposure to air for one week and one month, respectively, indicating that the framework of UTSA-120a can be retained.

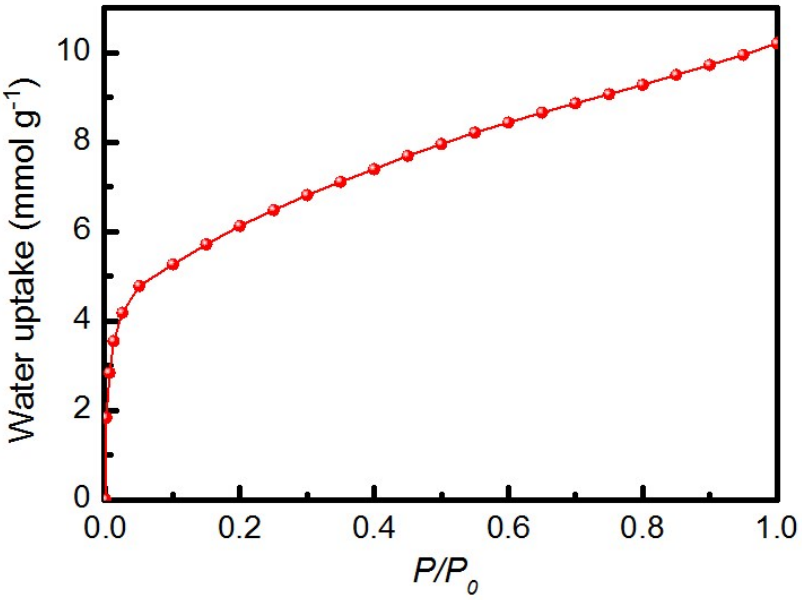

Figure S6. Water vapor sorption isotherms of UTSA-120a at room temperature.

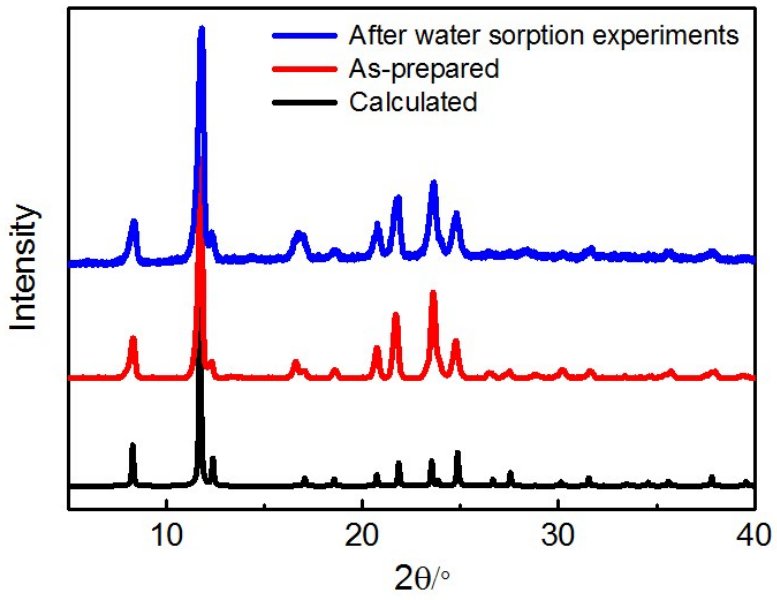

Figure S7. PXRD patterns of the UTSA-120a sample after water vapor sorption experiments, compared with the as-synthesized sample.

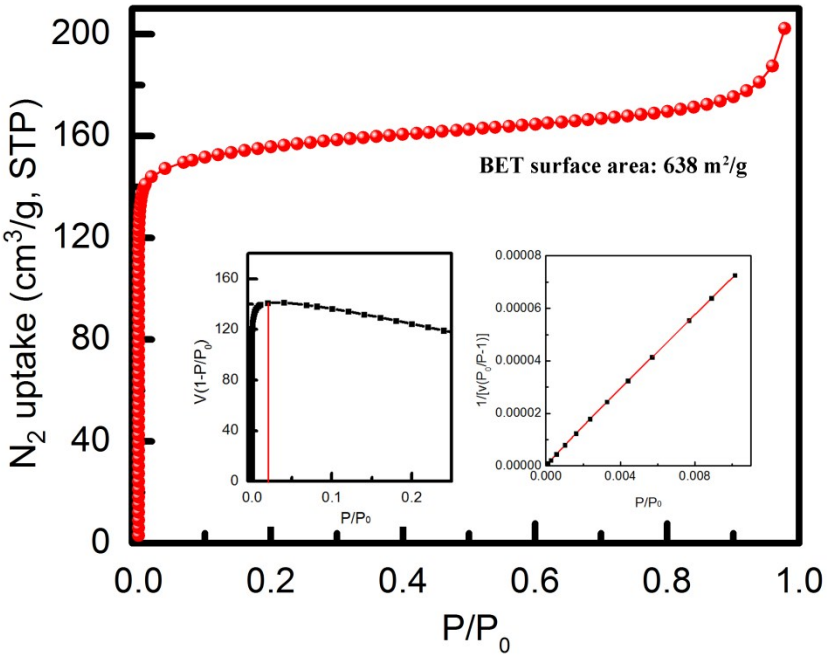

Figure S8. Nitrogen isotherm at 77 K with consistency and BET plots for the activated UTSA-120a sample.

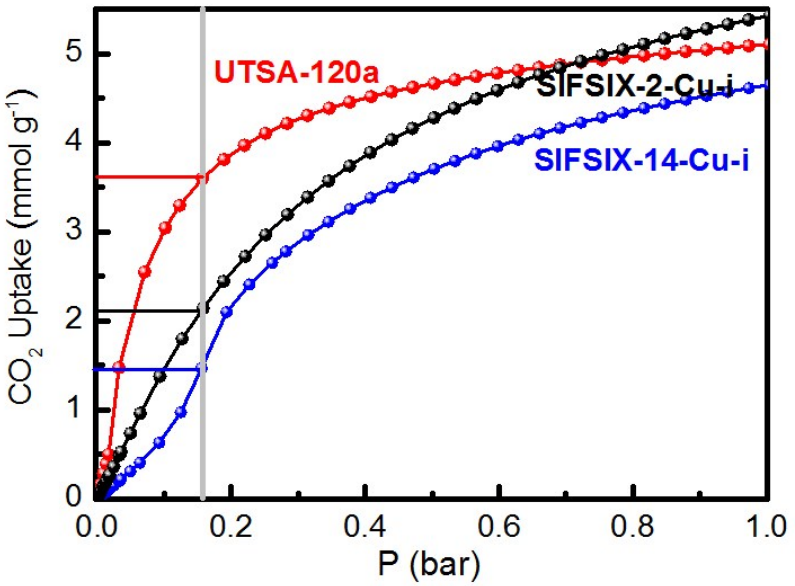

Figure S9. Comparison of CO_2 sorption isotherms and capture capacity (at 0.15 bar and room temperature) for UTSA-120a with SIFSIX-2-Cu-i and SIFSIX-14-Cu-i.

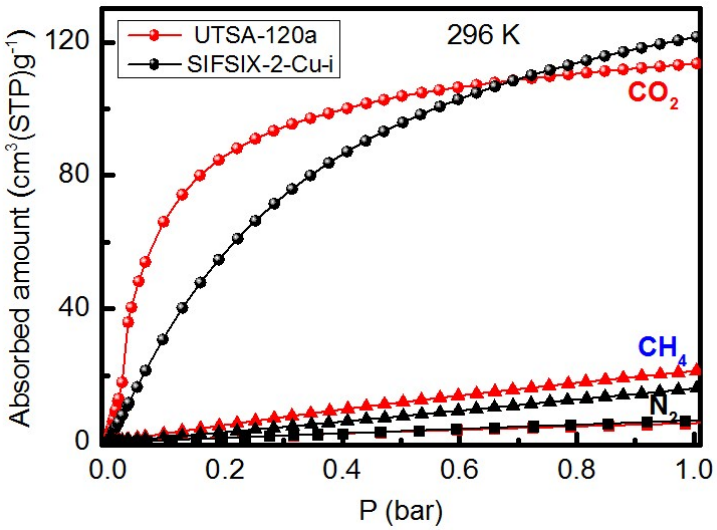

Figure S10. Adsorption isotherms of CO_4 (circles), CH_4 (triangles) and N_2 (squares) for UTSA-120a (red) and SIFSIX-2-Cu-i (black) at 296 K up to 1 bar.

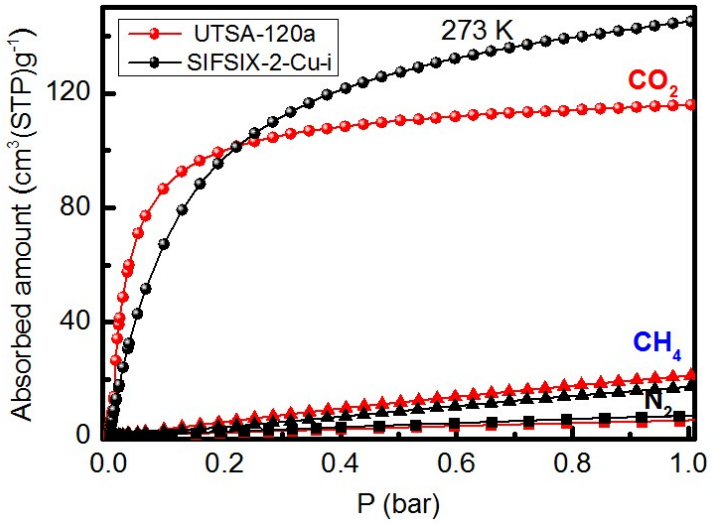

Figure S11. Adsorption isotherms of CO_4 (circle), CH_4 (triangle) and N_2 (square) for UTSA-120a (red) and SIFSIX-2-Cu-i (black) at 273 K up to 1 bar.

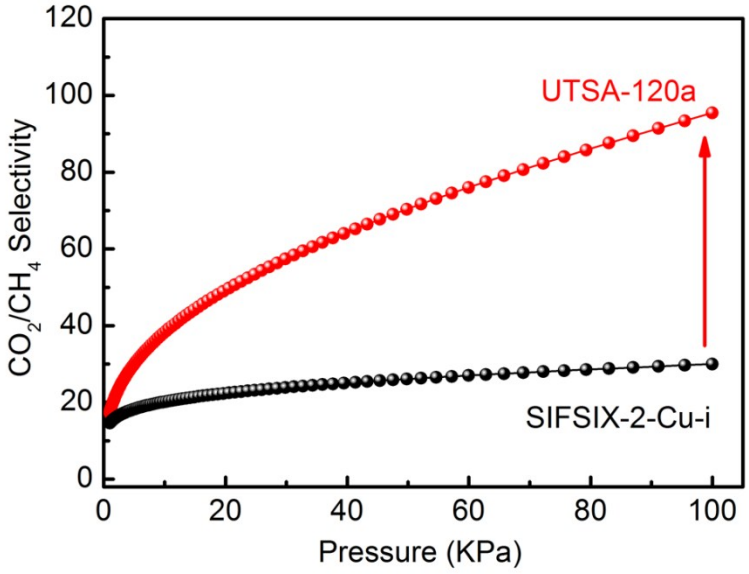

Figure S12. IAST selectivity of UTSA-120a (red) for CO_2/CH_4 (50/50, v/v) at 296 K, as compared with SIFSIX-2-Cu-i (black).

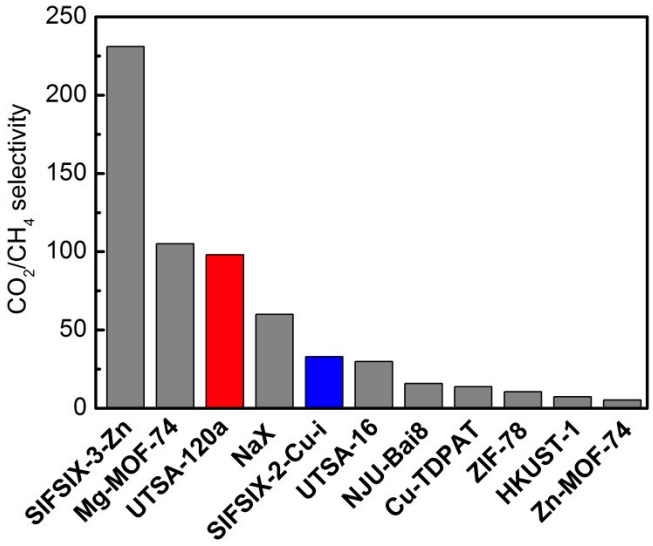

Figure S13. Comparison of IAST selectivity of UTSA-120a versus the other best-performing materials for CO_2/CH_4 (50/50) separation.

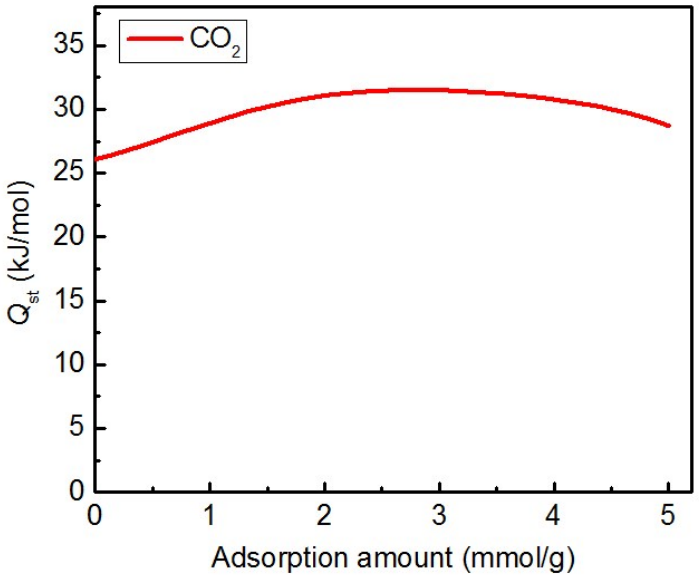

Figure S14. Heats of adsorption (Q_{st}) of CO_2 for UTSA-120a.

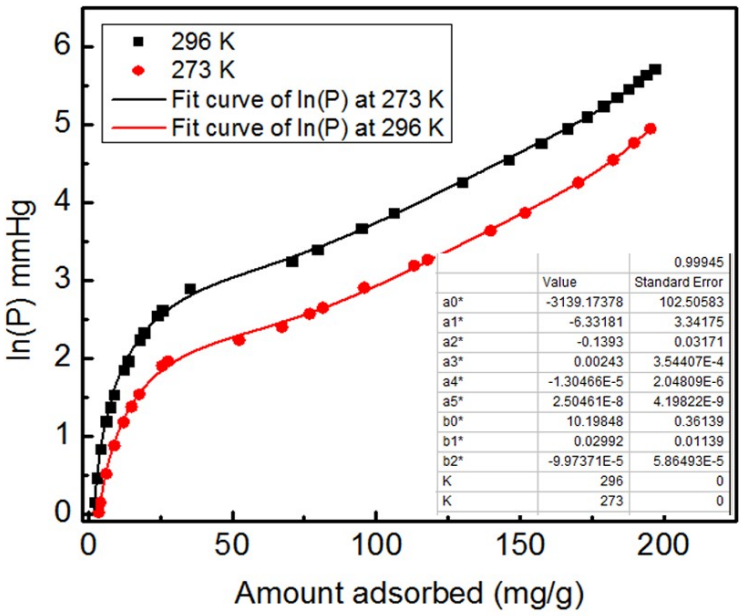

Figure S15. Virial fitting of the CO_2 adsorption isotherms for UTSA-120a.

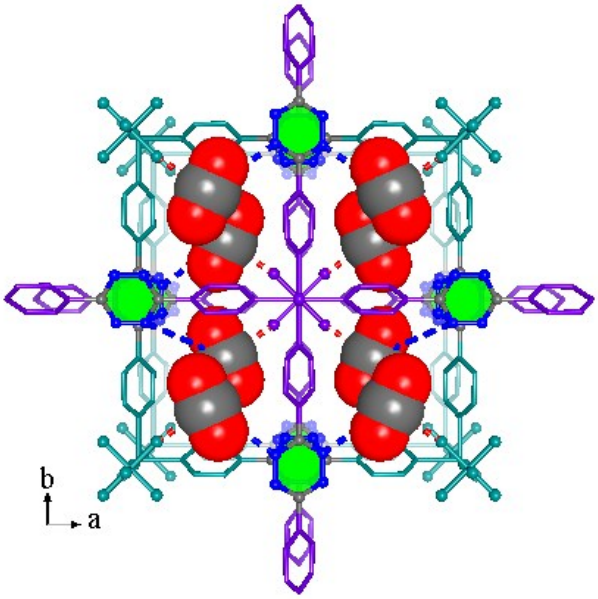

Figure S16. The binding sites and packing of CO_2 molecules in the channels of UTSA-120a, viewed along the *c* axis.

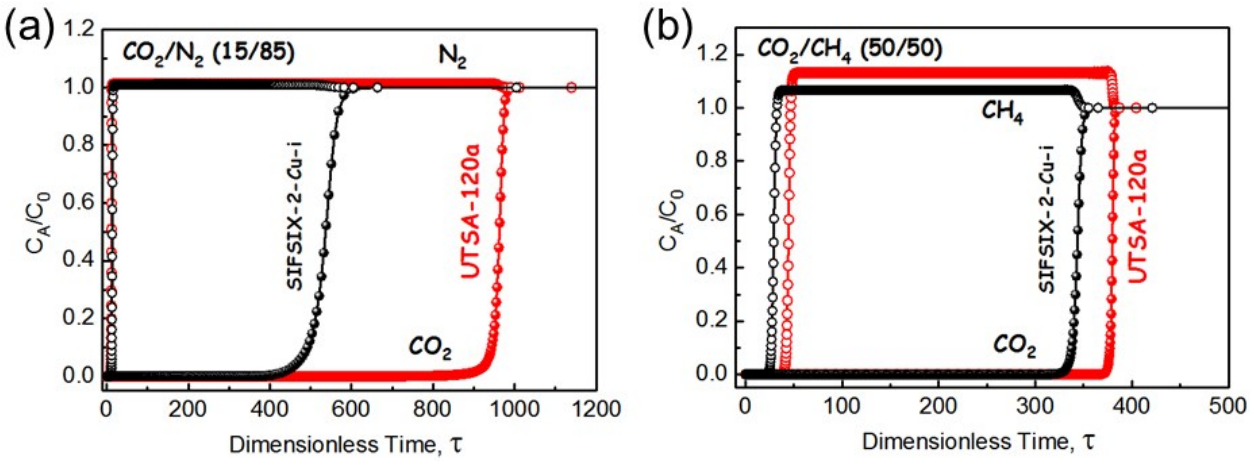

Figure S17. Transient breakthrough simulations of (a) CO_2/N_2 (15:85, v/v) mixture (b) CO_2/CH_4 (50:50) mixture on UTSA-120a versus SIFSIX-2-Cu-i at 298 K.

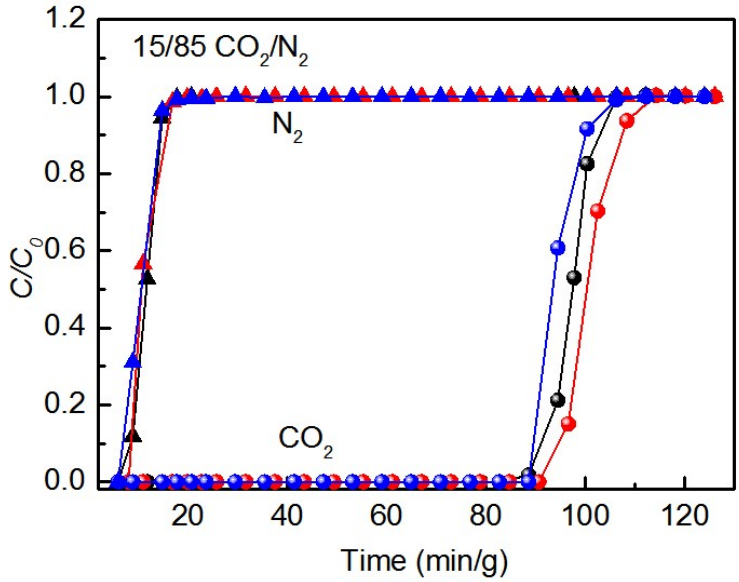

Figure S18. Cycling column breakthrough curves for CO_2/N_2 separation (15/85, v/v) with UTSA-120a at 298 K and 1.01 bar. The breakthrough experiments were carried out in a column packed with UTSA-120a (Φ 4.0 × 150 mm) at a flow rate of 2 mL/min.

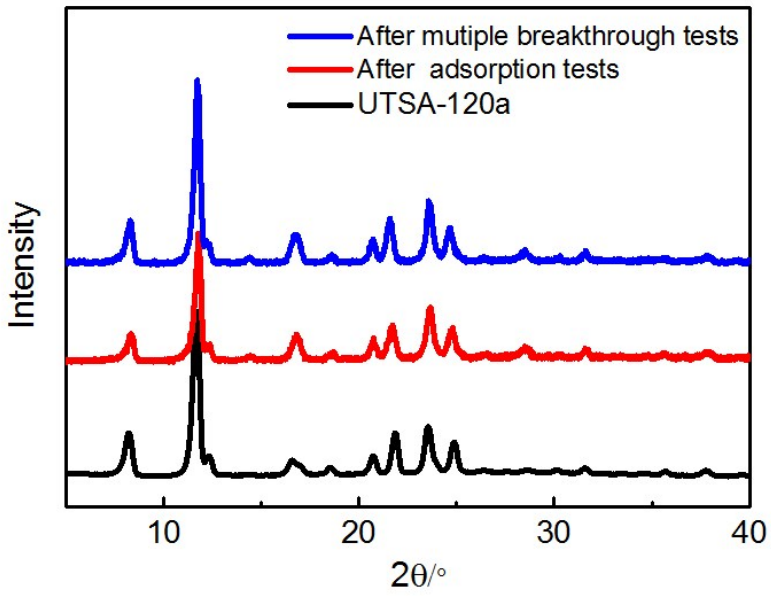

Figure S19. PXRD patterns of as-synthesized samples (black) and the samples after the adsorption tests (red) and multiple breakthrough tests (blue).

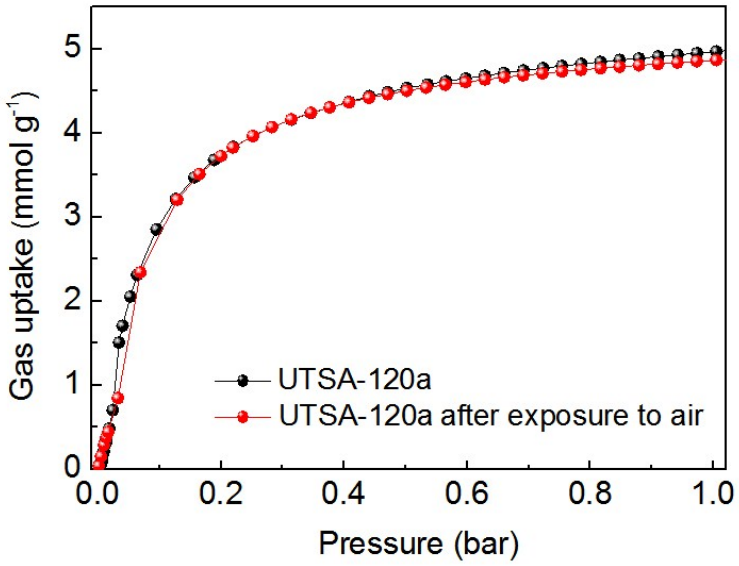

Figure S20. Comparison of CO_2 adsorption isotherms of UTSA-120a (black) and the re-activated sample after the exposure to air (red) for one week, confirming its good chemical stability.

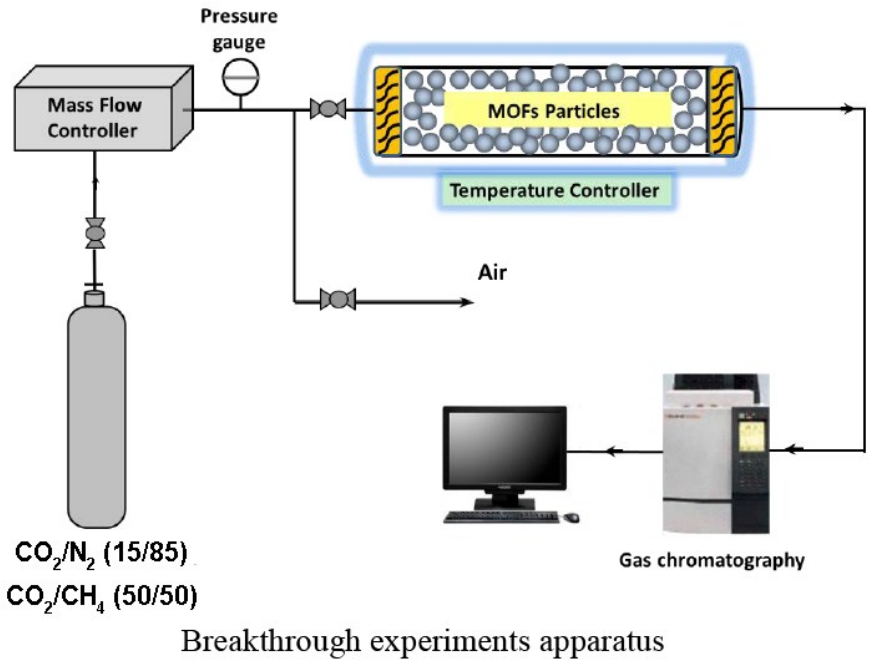

Figure S21. Schematic illustration of the apparatus for the breakthrough experiments.

References

[1] Krishna, R. The Maxwell-Stefan Description of Mixture Diffusion in Nanoporous Crystalline Materials. *Microporous Mesoporous Mater.* **2014**, *185*, 30-50.

[2] Krishna, R. Methodologies for Evaluation of Metal-Organic Frameworks in Separation Applications. *RSC Adv.* **2015**, *5*, 52269-52295.

[3] J. A. Mason, K. Sumida, Z. R. Herm, R. Krishna and J. R. Long, *Energy Environ. Sci.*, **2011**, *4*, 3030–3040.

[4] P.-Q. Liao, X.-W. Chen, S.-Y. Liu, X.-Y. Li, Y.-T. Xu, M. Tang, Z. Rui, H. Ji, J.-P. Zhang and X.-M. Chen, *Chem. Sci.*, **2016**, *7*, 6528–6533.

[5] P.-Q. Liao, H. Chen, D.-D. Zhou, S.-Y. Liu, C.-T. He, Z. Rui, H. Ji, J.-P. Zhang and X.-M. Chen, *Energy Environ. Sci.*, **2015**, *8*, 1011–1016.

[6] S. Xiang, Y. He, Z. Zhang, H. Wu, W. Zhou, R. Krishna and B. Chen, *Nat. Commun.*, **2012**, *3*, 954.

[7] T. M. McDonald, W. R. Lee, J. A. Mason, B. M. Wiers, C. S. Hong and J. R. Long, *J. Am. Chem. Soc.*, **2012**, *134*, 7056−7065.

[8] S. J. Datta, C. Khumnoon, Z. H. Lee, W. K. Moon, S. Docao, T. H. Nguyen, I. C. Hwang, D. Moon, P. Oleynikov, O. Terasaki and K. B. Yoon, *Science*, 2015, **350**, 302.

[9] A. Kumar, D. G. Madden, M. Lusi, K.-J. Chen, E. A. Daniels, T. Curtin, J. J. Perry IV and M. J. Zaworotko, *Angew. Chem., Int. Ed.*, **2015**, *54*, 14372−14377.

[10] O. Shekhah, Y. Belmabkhout, Z. Chen, V. Guillerm, A. Cairns, K. Adil and M. Eddaoudi, *Nat. Commun.*, **2014**, *5*, 4228.

[11] P. Nugent, Y. Belmabkhout, S. D. Burd, A. J. Cairns, R. Luebke, K. Forrest, T. Pham, S. Ma, B. Space, L. Wojtas, M. Eddaoudi and M. J. Zaworotko, *Nature*, **2013**, *495*, 80−84.

[12] A. Demessence, D. M. D'Alessandro, M. L. Foo and J. R. Long, *J. Am. Chem. Soc.*, 2009, **131**, 8784.

[13] P. M. Bhatt, Y. Belmabkhout, A. Cadiau, K. Adil, O. Shekhah, A. Shkurenko, L. J. Barbour and M. Eddaoudi, *J. Am. Chem. Soc.*, 2016, **138**, 9301.

[14] R. Vaidhyanathan, S. S. Iremonger, G. K. H. Shimizu, P. G. Boyd, S. Alavi and T. K. Woo, *Science*, 2010, **330**, 650.

[15] S. Nandi, S. Collins, D. Chakraborty, D. Banerjee, P. K. Thallapally, T. K. Woo and R. Vaidhyanathan, *J. Am. Chem. Soc.*, **2017**, *139*, 1734−1737.

[16] M. Jiang, B. Li, X. Cui, Q. Yang, Z. Bao, Y. Yang, H. Wu, W. Zhou, B. Chen and H. Xing, *ACS Appl. Mater. Interfaces*, 2018, **10**, 16628.

[17] J. An, S. J. Geib and N. L. Rosi, *J. Am. Chem. Soc.* **2010**, *132*, 38–39.

[18] Q.-G. Zhai, X. Bu, C. Mao, X. Zhao, L. Daemen, Y. Cheng, A. J. Ramirez-Cuesta and P. Feng, *Nat. Commun.*, **2016**, *7*, 13645.

[19] L. Du, Z. Lu, K. Zheng, J. Wang, X. Zheng, Y. Pan, X. You and J. Bai, J. Am. Chem. Soc., 2013, 135, 562–565.

[20] K.-J. Chen, D. G. Madden, T. Pham, K. A. Forrest, A. Kumar, Q.-Y. Yang, W. Xue, B. Space, J. J. Perry IV, J.-P. Zhang, X.-M. Chen and M. J. Zaworotko, *Angew. Chem. Int. Ed.*, **2016**, *55*, 10268–10272.

[21] J.-R. Li, J. Yu, W. Lu, L.-B. Sun, J. Sculley, P. B. Balbuena and H.-C. Zhou, *Nat. Commun.*, **2013**, *4*, 1538.

[22] B. Li, Z. Zhang, Y. Li, K. Yao, Y. Zhu, Z. Deng, F. Yang, X. Zhou, G. Li, H. Wu, N. Nijem, Y. J. Chabal, Z. Lai, Y. Han, Z. Shi, S. Feng and J. Li, *Angew. Chem. Int. Ed.*, **2012**, *51*, 1412–1415.

[23] F. Luo, C. Yan, L. Dang, R. Krishna, W. Zhou, H. Wu, X. Dong, Y. Han, T.-L. Hu, M. O'Keeffe, L. Wang, M. Luo, R.-B. Lin and B. Chen, *J. Am. Chem. Soc.*, **2016**, *138*, 5678−5684.